Swiss Journal of Palaeontology (2026) 145: 943–956 | DOI 10.3897/sjp.145.207461

PENSOFT

Swiss Journal of Palaeontology SGG SGS scnat swiss academy of sciences

Research Article

A near-complete caudipterid pes from the Early Cretaceous Jehol Biota reveals insights into pedal anatomy and osteohistology of early oviraptorosaurs

Mengxi Han[1*], Menghan Duan[1,2*], Jingyao Song[1], Mingze Hao[3,4], Yujie Liu[1], Shuai Shao[1], Kohta Kubo[5], Yang Li[1], Qian Wu[3], Paul Rummy[3], Shiying Wang[1]

1 *College of Paleontology, Shenyang Normal University, Shenyang, 110034, China*
2 *School of Earth and Planetary Sciences, China University of Geosciences, Wuhan, 430074, China*
3 *Key Laboratory of Vertebrate Evolution and Human Origins of Chinese Academy of Sciences, Institute of Vertebrate Paleontology and Paleoanthropology, Chinese Academy of Sciences, Beijing, 100044, China*
4 *College of Earth and Planetary Sciences, University of Chinese Academy of Sciences, Beijing, 100049, China*
5 *Department of Earth and Planetary Science, Graduate School of Science, The University of Tokyo, Tokyo, 113-0033, Japan*

https://zoobank.org/A1332B1B-B740-4E44-8E61-91310FCE4E9B

Corresponding author: Shiying Wang (wang-shiying@outlook.com)

Academic editor: Emanuel Tschopp ♦ **Received** 12 July 2026 ♦ **Accepted** 9 September 2026 ♦ **Published** 25 September 2026

Abstract

The evolution of the pedal morphology and the ontogeny of early oviraptorosaur theropods remain inadequately understood, largely owing to the poor preservation of available material and the limitations of traditional observation methods. Here, we describe a particularly well-preserved and nearly complete pedal specimen (PMOL-AD00126) from the Lower Cretaceous Jehol Group of western Liaoning, P.R. China and assign it to Caudipteridae, an early-diverging clade of oviraptorosaurs. Three-dimensional reconstruction of the pes reveals numerous previously undocumented morphological features, including a subarctometatarsalian metatarsus, metatarsal I with pronounced dorsal and plantar prominences, distinct plantar ridges on metatarsals II and III, an elongated extensor ligament pit on metatarsal III and well-developed extensor ligament pits and articular ridges on the pedal phalanges. Histological analysis indicates that this individual had not attained complete somatic maturity. These newly-recognised morphological and histological characters provide significant insights not only into the taxonomy and ontogeny of Caudipteridae, but also into the evolution of early oviraptorosaurs.

Keywords

Caudipteridae, Jehol Biota, metatarsus, osteohistology, Oviraptorosauria, three-dimensional reconstruction

Introduction

Oviraptorosauria is a highly specialised clade of non-avialan theropod dinosaurs, with a fossil record primarily spanning the Cretaceous of Asia and North America (Zhou and Wang 2000; Wang et al. 2013; Funston et al. 2018; Hao et al. 2025). This group is pivotal for understanding the origin of birds, exhibiting numerous bird features, including pennaceous feathers, a pygostyle-like structure and preserving evidence of brooding behaviour (Ji et al. 1998; Zhou et al. 2000; He et al. 2008; Qiu et al. 2019; Bi et al. 2021). Notably, early-diverging

* These authors contributed equally.

oviraptorosaurs from the Early Cretaceous are currently known almost exclusively from the Jehol Biota in western Liaoning, China. To date, seven species across six genera of early-diverging oviraptorosaurs have been recovered from the Jehol Biota. Of these, *Caudipteryx zoui*, *Caudipteryx dongi*, *Similicaudipteryx yixianensis* and *Xingtianosaurus ganqi* are assigned to Caudipteridae, a family erected by Zhou and Wang (2000) and phylogenetically defined by Hendrickx et al. (2015) as the most inclusive clade containing *Caudipteryx zoui*, but excluding *Oviraptor philoceratops* and *Caenagnathus collinsi*. The remaining three non-caudipterid species are *Protarchaeopteryx robusta*, *Incisivosaurus gauthieri* and *Ningyuansaurus wangi*. These taxa provide crucial insights into the early evolution of the group.

However, despite their frequently exquisite preservation, the detailed pedal anatomy of Jehol oviraptorosaurs remains poorly documented. This is largely due to the preservation of most specimens in slabs. This preservation mode obscures or distorts critical features such as metatarsal arrangement, thereby limiting broader understanding of pedal evolution within Oviraptorosauria (Ji et al. 2012; Qiu et al. 2019; Hao et al. 2025). In parallel, osteohistological research on oviraptorosaurs is largely concentrated in the derived clades Caenagnathidae and Oviraptoridae, whereas data from early-diverging taxa remain extremely scarce. Currently, osteohistological data for Jehol oviraptorosaurs are limited. Only osteohistological data from the femur of *Caudipteryx zoui* (IVPP 11819) and from the fibula of *Similicaudipteryx yixianensis* (PMOL-AD00113) have been reported; however, the accompanying descriptions are limited in detail (Erickson et al. 2009; Cullen et al. 2020). This paucity of data constitutes a critical gap in our understanding of the ontogenetic status and osteohistological variation of early oviraptorosaurs.

To address these recognised gaps in both morphological and osteohistological data, we present a detailed anatomical description, facilitated by CT scanning and three-dimensional reconstruction, alongside a histological analysis of a nearly complete caudipterid pes. These new data collectively refine the taxonomic and ontogenetic understanding of Caudipteridae and illuminate the early evolution of pedal morphology in oviraptorosaurs.

Materials and methods

Material

PMOL-AD00126 is a left articulated pes from western Liaoning, P.R. China and is housed at the Paleontological Museum of Liaoning (PMOL) (Fig. 1). As the specimen was acquired by the museum, precise locality and horizon data are unavailable. Given the lithology of its matrix, the specimen is considered to have been recovered from the Yixian Formation.

The terminal phalanges of pedal digits II–IV are missing, but their impressions are well preserved on the matrix. To mitigate this loss, previous preparators prepared epoxy-resin casts from these impressions and these casts have allowed us to determine some anatomical information.

Methods

CT scanning and segmentation

Micro-computed tomography (micro-CT) scanning of the specimen was performed using a GE Phoenix v|tome|x m300 & 180 micro-CT scanner (GE Measurement & Control Solutions, Wunstorf, Germany) at the High-Resolution X-ray Computed Tomography Laboratory, Institute of Vertebrate Paleontology and Paleoanthropology, Chinese Academy of Sciences, Beijing, China. Scanning was performed at 180 kV and 130 μA, yielding a resolution of 58.54496 μm per pixel. The CT data were imported into Mimics 19.0 (Materialise, Leuven, Belgium; https://www.materialise.com) for segmentation. Individual pedal elements were segmented manually by slice-by-slice editing. The segmented models were then exported to Blender 4.5 for visualisation and post-segmentation processing. Specifically, small isolated fragments and high-density mineral grains were removed and minor smoothing and hole filling were applied to improve the visual continuity of the models. These procedures were restricted to surface cleaning and did not alter diagnostic osteological features, articular morphology or the relative positions of the preserved elements. The micro-CT image stack (TIFF) and segmented three-dimensional models of the individual pedal elements (STL) are deposited in ScienceDB at https://www.scidb.cn/anonymous/WVozWW55.

Histological sampling and preparation

Although metatarsals are not commonly used as histological material for assessing ontogenetic stages, previous histological studies have demonstrated that metatarsal II constitutes suitable material for investigating pedal growth and development in theropods, as exemplified by caenagnathid TMP 1990.52.10 (Voris et al. 2024) and *Xixianykus zhangi* (Qin et al. 2019). Metatarsal II was selected because it alone retains an intact diaphyseal wall through the mid-distal portion, permitting a complete transverse section that yields a full histological record of bone growth and remodelling. In contrast, metatarsal III is strongly pinched and the mid-shaft of metatarsal IV is heavily damaged.

Thin sections were prepared following standard histological procedures (Padian and Lamm 2013). The sampling site has been restored with epoxy resin. The metatarsal II sample was embedded in EXAKT Technovit

7200 resin and cured for 12 hours. Following protocols commonly employed in previous studies (Wu et al. 2021; Wu et al. 2024; Wu et al. 2025), the embedded block was transversely sectioned perpendicular to the bone's long axis using an SPQJ-300 slicing machine and the cut surface was subsequently ground and polished with an SPM-300A grinding and polishing machine until optimal optical contrast was achieved. Without post-section repair or other chemical treatments, the sections were directly examined under a Nikon Eclipse LV100NPOL microscope with both normal light and polarised light and photographed with a DS-Fi3 camera and the built-in NIS-Element v4.60 software.

Results

Morphological description

Tarsals

The proximal tarsals are heavily damaged and disarticulated from the rest of the pes (Fig. 1). Three small distal tarsal fragments are in close contact with the proximal metatarsals, though unfused to each other or to the metatarsals. This condition contrasts with that observed in *Avimimus*, *Yuanyanglong* and some caenagnathids (e.g. *Citipes elegans*), in which the distal tarsals are fused to the proximal ends of the metatarsals (Currie 1989; Vickers-Rich et al. 2002; Funston et al. 2016; Hao et al. 2025).

Metatarsals

The proximal and distal ends of the metatarsals are unfused. Metatarsal I has a proximally tapering shaft and a bulbous distal head, separated by a weakly constricted neck (Fig. 2M–Q). The length ratio of metatarsal I to metatarsal II is approximately 0.19, similar to the condition in *Similicaudipteryx yixianensis* (0.17) and *Citipati osmolskae* (0.21) (He et al. 2008; Wang et al. 2013), slightly greater than that of *Caudipteryx zoui* (0.16) (Zhou et al. 2000), but substantially lower than in other oviraptorids such as *Ganzhousaurus nankangensis* (0.29) (Wang et al. 2013) and *Khaan mckennai* (0.26) (Balanoff and Norell 2012). Metatarsal I attaches to the ventromedial surface of metatarsal II. Its proximal end is located at approximately the distal third of metatarsal II, a position comparable to that in *Similicaudipteryx yixianensis* (He et al. 2008). In dorsal view, the proximal half of metatarsal I has a relatively straight medial margin and lacks significant torsion along its longitudinal axis (Fig. 2M). The distal half curves slightly medially, forming a gently concave medial margin, a condition similar to that in *Khaan mckennai* (Balanoff and Norell 2012). In contrast, the medial margin of *Citipati osmolskae* is more markedly concave (Hattori 2016). The mid-shaft of metatarsal I bears pronounced dorsal and ventral prominences (Fig. 2O, P). The size of these prominences is comparable to that in *Chirostenotes pergracilis* and *Anzu wyliei* (Yun and Funston 2021). However, more pronounced prominences are present in *Citipati osmolskae* (Hattori 2016). In contrast, such prominences are absent in dromaeosaurids (e.g. *Deinonychus antirrhopus*) and troodontids (e.g. *Talos sampsoni*) (Hattori 2016; Yun and Funston 2021). The articular surface for metatarsal II is proximodistally elongated, spanning approximately half the length of metatarsal I (Fig. 2P). In lateral view, the articular surface exhibits a teardrop-shaped outline, gradually widening towards the distal end. It features a broad, shallow depression along its proximodistal axis. Distally, the lateral collateral ligament fossa is large, deep and ovoid in shape and is positioned close to the distal margin. This condition resembles that of *Microvenator celer*, *Rinchenia mongoliensis* and *Citipati osmolskae*, but differs from the kidney-shaped and more proximally positioned fossa in *Chirostenotes pergracilis* (Hattori 2016; Yun and Funston 2021). The medial collateral ligament fossa of PMOL-AD00126 is a poorly defined, shallow depression**,** a condition similar to that in the oviraptorid *Citipati osmolskae*, but contrasting with the well-developed medial fossa observed in the caenagnathid *Chirostenotes pergracilis* (Hattori 2016; Yun and Funston 2021). In dorsal view, the distal articular surface of metatarsal I is ball-shaped (Fig. 2S). Its plantar surface is separated by a shallow, wide intercondylar groove, akin to that of an indeterminate caenagnathid (UW 44439) and *Anzu wyliei* (Yun and Funston 2021). In contrast, the intercondylar groove in *Citipati osmolskae* is considerably deeper (Hattori 2016).

Metatarsal II is slightly shorter than metatarsals III and IV, measuring approximately 0.93 times the length of metatarsal III (Table 1). This proportion is closer to that of *Caudipteryx zoui* (~0.9) and slightly exceeds that of *Similicaudipteryx yixianensis* (PMOL-AD00113, 0.87) (Zhou and Wang 2000; Liu 2014). Proximally, metatarsal II aligns with metatarsal IV and both extend slightly more proximally than metatarsal III. Distally, metatarsal II reaches the proximal margin of the medial collateral ligament fossa of metatarsal III. The proximal end of metatarsal II is markedly mediolaterally widened (Fig. 2R), similar to that of other caudipterids, such as the holotype of *Xingtianosaurus ganqi* (Qiu et al. 2019). The shaft of the metatarsal II is straight, whereas its distal portion curves slightly medially, deviating the distal end away from metatarsal III (Fig. 2A). The articular surface for metatarsal I is a shallow depression on the distal third of metatarsal II. Proximally, this depression is located on the medial surface of metatarsal II, whereas, distally, it extends onto the plantar surface (Fig. 2B, C). The shaft of metatarsal II bears a well-developed posteromedial ridge that extends plantarly to approximately the level of the plantar margin of the distal condyle (Fig. 2B).

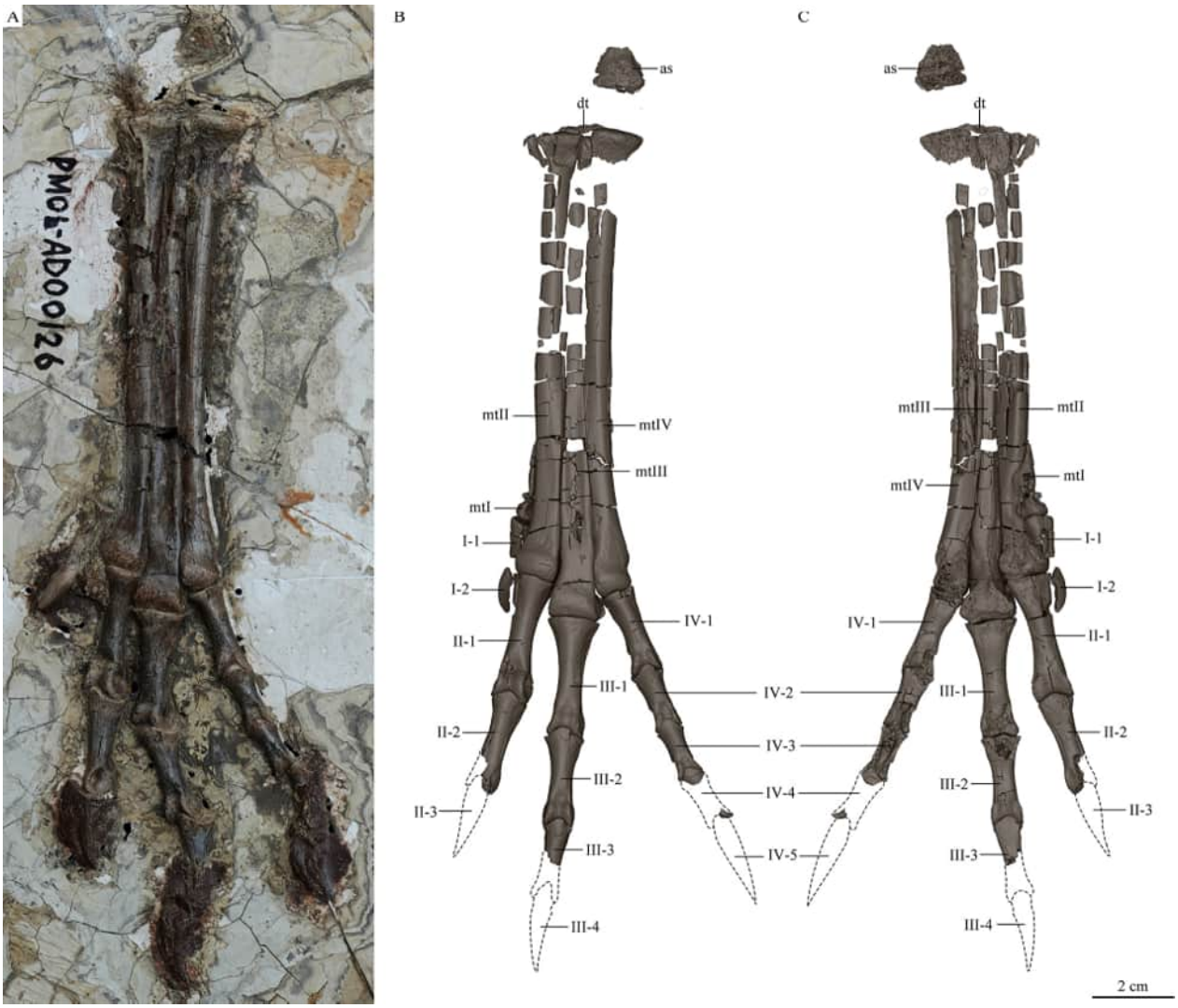

Figure 1. Left foot of referred specimen of Caudipteridae, PMOL-AD00126. Photograph (**A**); digital reconstruction in dorsal (**B**) and plantar (**C**) views. Dotted lines indicate the reconstructed outlines of the bones. Abbreviations: as, astragalus; dt, distal tarsal; mtI to mtIV, metatarsals I to IV; I-1 to IV-5, pedal phalanges I-1 to IV-5.

The collateral ligament fossae are well developed, with the medial fossa more rounded than the lateral fossa (Fig. 2C, D). The plantar surfaces of the distal end are divided by a shallow, wide intercondylar groove. The lateral condyle is slightly larger than the medial condyle. In contrast, many caenagnathids possess a deeper intercondylar groove and a lateral condyle that is considerably larger than the medial condyle (e.g. *Caenagnathus collinsi*) (Funston et al. 2015).

Metatarsal III is strongly pinched. The proximal end of metatarsal III is fully exposed dorsally, forming a subarctometatarsalian condition (Fig. 2E). In the anteroposterior direction, the bone is thinnest at the mid-shaft, with a thickness of 1.74 mm. Distally, the shaft gradually thickens and the medullary cavity expands. A distinct neck is present proximal to the articular head. An elongate depression extends longitudinally from the dorsal surface of the mid-shaft to the neck, which is positioned just proximal to the articular head of metatarsal III. This feature is similar to that observed in *Neuquenraptor argentinus* (Brissón Egli et al. 2017) and likely represents the insertion area of the *M. extensor brevis digiti III* (White et al. 2016). The plantar surface of the shaft bears two longitudinal ridges (Fig. 2F), a feature previously documented only in Caenagnathidae amongst coelurosaurian lineages that possess an arctometatarsus (Funston et al. 2016; Tsujimura et al. 2021). As in *Anzu wyliei* and *Chirostenotes pergracilis* (TMP 1979.020.0001), these ridges are not continuous with the condylar ridges, a condition that contrasts with that observed in *Anomalipes zhaoi*, *Eoneophron infernalis*, *Elmisaurus rarus* and *Citipes elegans* (Currie et al. 2016; Funston et al. 2016; Yu et al. 2018; Funston 2020; Atkins-Weltman et al. 2024). Metatarsal III is slightly deflected medially at the distal neck, resulting in a slight medial inclination of the distal articular surface. The collateral ligament fossae are subequal in size and symmetrically positioned. In distal view, the articular surface for phalanx III-1 is transversely broad and nearly rectangular. The intercondylar groove is shallow and restricted to the plantar surface and the medial condyle is slightly larger than the lateral condyle.

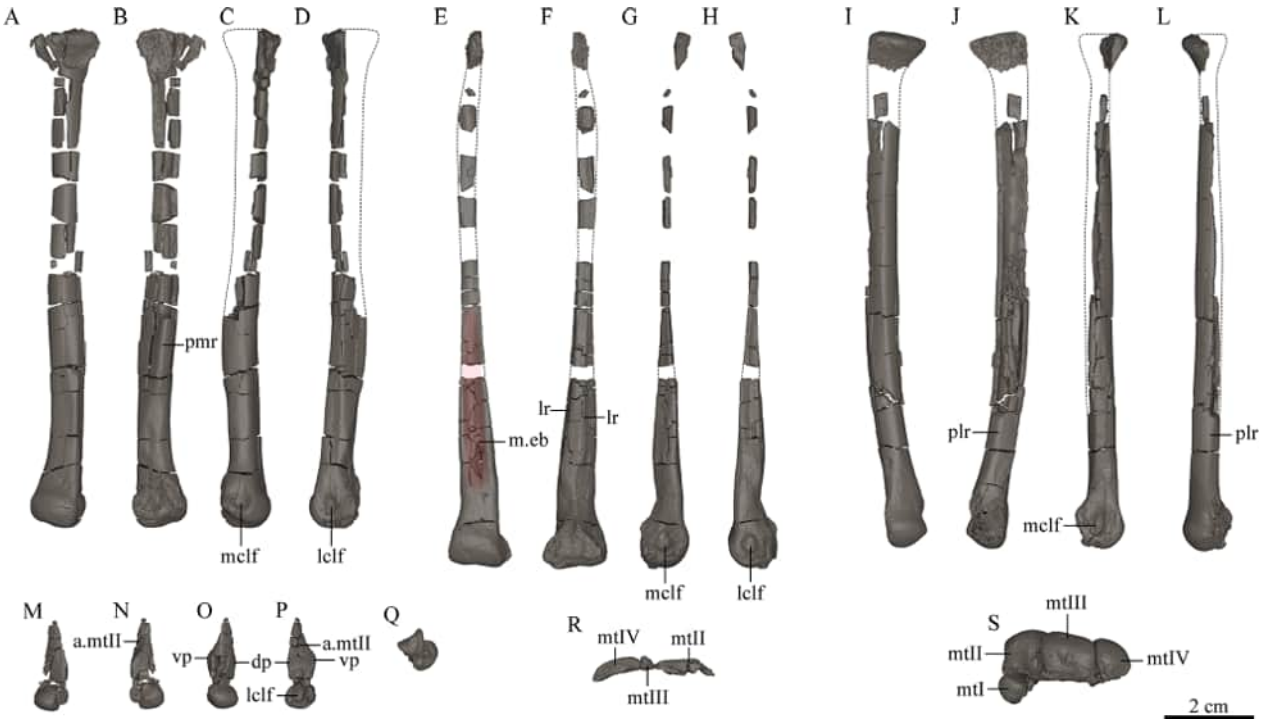

Figure 2. Digital reconstructions of the metatarsals of referred specimen of Caudipteridae, PMOL-AD00126. Metatarsal II in dorsal (**A**), plantar (**B**), medial (**C**) and lateral (**D**) views; metatarsal III in dorsal (**E**), plantar (**F**), medial (**G**) and lateral (**H**) views; metatarsal IV in dorsal (**I**), plantar (**J**), medial (**K**) and lateral (**L**) views; metatarsal I in dorsal (**M**), plantar (**N**), medial (**O**), lateral (**P**) and proximal (**Q**) views; articulated metatarsals II–IV in proximal view (**R**); articulated metatarsals I–IV in distal view (**S**). Dotted lines indicate the reconstructed outlines of the bones; the red area in (E) indicates muscle attachment regions. Abbreviations: a. mtII, articular facets for metatarsal II; dp, dorsal prominence; lclf, lateral collateral ligament fossa; lr, longitudinal ridge; mclf, medial collateral ligament fossa; m. eb, attachment area for m. extensor brevis digiti III; mtI to mtIV, metatarsals I to IV; plr, posterolateral ridge; pmr, posteromedial ridge; vp, ventral prominence.

Table 1. Measurements of PMOL-AD00126 and other early-diverging oviraptorosaurs from the Jehol Biota.

Group	Taxon	MT I	MT II	MT III	MT IV	I-1	I-2	II-1	II-2	II-3	III-1	III-2	III-3	III-4	IV-1	IV-2	IV-3	IV-4	IV-5	References
Caudipterids	**PMOL-AD00126[a]**	20.5	110.5	118.5	115.1	14.2*	13.7	31.3	25.4	20.7*	29.4	24.3	21.5*	22.7*	21.0	17.1	15.7	16.1*	19.8*	This study
	IVPP V 12556 *Similicaudipteryx yixianensis*	25.0	144.0	183.0*	153.0	28.0	23.0	43.0	39.0	33.0*	46.0	34.0	32.0	34.0	30.0	23.0	18.0	21.0	20.0	He et al. (2008)
	IVPP V 13390 *Xingtianosaurus ganqi*	9.8	80.4	89.7	82.8	19.0	14.6	28.3	22.3	–	27.0	20.9	20.3	17.2	17.3	14.5	12.7	16.0	16.0	Qiu et al. (2019)
	BPM 0001 *Caudipteryx zoui*	16.0	102.0	113.0	107.0	13.0	12.0	23.0	16.0	19.0	24.0	19.0	15.0	18.0	14.0	8.0	6.0	4.0	14.0	Zhou et al. (2000)
	IVPP V 12344 *Caudipteryx dongi*	19.0	112.0	124.0	116.0	12.0	11.0	25.0	16.0	19.0	27.0	20.0	17.0	20.0	15.0	9.0	7.0	7.0	16.0	Zhou and Wang (2000)
	IVPP V 12430 *Caudipteryx*	15.0	102.0	112.0	106.0	12.0	12.0	22.0	14.0	17.0	23.0	17.0	13.0	18.0	12.0	8.0	6.0	5.0	14.0	Zhou et al. (2000)
Non-caudipterid oviraptorosaurians	*Ningyuansaurus wangi*	–	88.0	105.0	102.0	–	–	–	–	–	24.0	–	–	–	–	–	–	–	–	Ji et al. (2012)
	GMV 2125 *Protarchaeopteryx robusta*	13.0	77.0	86.0	81.0	–	–	–	–	–	–	–	–	–	–	–	–	–	–	Ji and Ji (1997)

All measurements are in millimetres. Abbreviations: MT, metatarsal. Symbols: *, estimated value. [a] PMOL-AD00126 is provisionally referred to Caudipteridae.

Metatarsal IV is slightly curved laterally along its length (Fig. 2I). The proximal end is expanded laterally. The plantar surface of the shaft bears a weakly developed posterolateral ridge (Fig. 2J). Proximal to the distal articulation, the dorsolateral surface of the distal portion of the shaft exhibits a slight medial concavity, similar to that observed in *Avimimus* (Funston et al. 2019). The distal articulation for phalanx IV-1 is roughly ball-shaped. The medial collateral ligament fossa is well developed and the medial condylar ridge extends plantarly considerably beyond the shaft. The lateral collateral ligament fossa, lateral condyle and intercondylar groove are not preserved due to damage.

Metatarsal V is not preserved.

Phalanges

The preserved pedal phalanges comprise I-1 to I-2, II-1 to II-2, III-1 to III-3 and IV-1 to IV-4. Based on the preserved phalanges and impressions of the missing unguals II to IV, the phalangeal formula is 2-3-4-5.

Phalanx I-1 has a single concave proximal articular surface that lacks a distinct ridge, forming a ball-and-socket joint with the distal end of the metatarsal I (Fig. 3E). The proximal end is relatively robust and gradually tapers towards the mid-shaft (Fig. 3A). Phalanx I-2 (ungual) is partially preserved, but bears a well-developed extensor tubercle (Fig. 3C).

Phalanx II-1 is the longest phalanx, with a length ratio of approximately 1.06 relative to that of phalanx III-1. This condition resembles that of *Xingtianosaurus ganqi*, but differs from the condition in other known caudipterids, in which phalanx II-1 is slightly shorter than phalanx III-1 (Zhou and Wang 2000; Zhou et al. 2000; Liu 2014; Qiu et al. 2019). The proximal articular surface of phalanx II-1 is a single concave facet without a distinct ridge (Fig. 3J). In proximal view, this surface is dorsoplantarly tall, with its height significantly exceeding its mediolateral width. The plantar margin of the proximal end bears a low flexor tubercle. The dorsal margin of the proximal end is convex, but lacks a distinct extensor tubercle, a condition similar to that observed in *Khaan mckennai* and *Elmisaurus rarus* (Osmólska 1981; Balanoff and Norell 2012). The plantar surface of the shaft is relatively flat (Fig. 3G), resembling that of other oviraptorosaurs (Tsogtbaatar et al. 2022). The dorsal surface bears a well-developed, elliptical extensor pit, which is notably deeper than the corresponding structures on other phalanges. This fossa is situated closer to the medial margin of the shaft and is nearly confluent with the prominent intercondylar groove (Fig. 3F). By contrast, in the oviraptorid *Khaan mckennai* and the caenagnathid *Elmisaurus rarus*, the fossa is shallower (Osmólska 1981; Balanoff and Norell 2012); in the caenagnathid *Citipes elegans*, the dorsal surface of this region is relatively flat and lacks a distinct extensor pit (Funston et al. 2016). The collateral ligament fossae on either side of phalanx II-1 differ markedly in morphology. The lateral collateral ligament fossa is small and rounded, with steeply sloping and well-defined margins and is positioned roughly equidistant from the dorsal and plantar margins of the lateral articular condyle (Fig. 3I). The medial fossa, in contrast, is larger and proximodistally elongated, with gently sloping margins and is located closer to the plantar margin of the medial articular condyle (Fig. 3H). The distal articulation of phalanx II-1 is well ginglymoid with a deep intercondylar groove. The lateral condyle is distinctly larger than the medial condyle (Fig. 3J). The shaft of phalanx II-2 tapers gradually towards the distal end (Fig. 3F). The proximal articular surface is roughly oval and is divided into two asymmetrical facets by a prominent ridge that extends obliquely from dorsomedial to plantarolateral (Fig. 3J). The lateral facet is larger and extends further plantarwards than the medial facet. The extensor tubercle and the flexor tubercle of phalanx II-2 are well developed, with the extensor tubercle projecting more proximally than the flexor tubercle (Fig. 3I), a condition similar to that in *Citipes elegans* (Funston et al. 2016). The lateral collateral ligament fossa has a proximodistally elongated and oval shape and is positioned closer to the dorsal margin of the lateral condyle. The intercondylar groove is well developed (Fig. 3J). The cast of phalanx II-3 (ungual) indicates that this element is short, robust and bears a lateral longitudinal vascular groove.

Phalanx III-1 bears a single, shallow, oval proximal articular surface (Fig. 3O). The dorsoplantar height of this surface is notably less than its mediolateral width. The lateral and medial margins of the proximal articulation of phalanx III-1 are nearly straight in lateral or medial view, a condition resembling that of phalanx III-1 in *Similicaudipteryx yixianensis*; by contrast, in *Caudipteryx dongi*, the proximal articular margins of phalanx III-1 are concave (He et al. 2008). The shaft tapers markedly towards its middle portion and curves dorsally (Fig. 3M). The extensor pit of phalanx III-1 is markedly shallower than that of phalanx II-1 (Fig. 3K), a feature also observed in *Parvicursor remotus* (Averianov and Lopatin 2021). The collateral ligament fossae on both sides are deep, well-defined and oval in outline. The distal articulation is transversely expanded and strongly ginglymoid (Fig. 3O), with a deep, wide intercondylar groove. The lateral condyle is significantly larger than the medial condyle. The proximal articular surface of phalanx III-2 is divided into two asymmetrical concave facets by a shallow ridge (Fig. 3O). The proximal extensor tubercle is well developed, whereas the flexor tubercle is not preserved due to damage. The shaft of phalanx III-2 gradually tapers from the proximal end to its middle portion and is slightly curved dorsally (Fig. 3M). The extensor pit is deeper than in other phalanges, except for phalanx II-1. The collateral ligament fossae on both sides are deep with well-defined margins. The articulation is strongly ginglymoid, with a well-developed intercondylar groove. The lateral condyle is slightly larger than the medial condyle (Fig. 3O). The proximal articular surface of phalanx III-3 is elliptical in outline, with a low ridge dividing it into two concave facets. The lateral facet is slightly larger than the medial facet (Fig. 3O). Both the flexor tubercle and the extensor tubercle are well developed (Fig. 3M). The cast of phalanx III-4 (ungual) bears a lateral groove.

Digit IV is elongated, with a length ratio of 0.92 relative to digit III. Phalanx IV-1 bears a single, shallow proximal articular surface (Fig. 3T). The dorsoplantar height of this surface exceeds its mediolateral width. In proximal view, the medial margin of the articular surface is relatively straight, whereas the lateral margin curves laterally, resulting in a semicircular outline similar to that of *Anomalipes zhaoi* (Yu et al. 2018). The extensor tubercle is weakly developed. In dorsal view, the lateral margin of the shaft of phalanx IV-1 is relatively straight, whereas the medial margin is slightly concave. Distally, the extensor pit is the shallowest amongst all the preserved

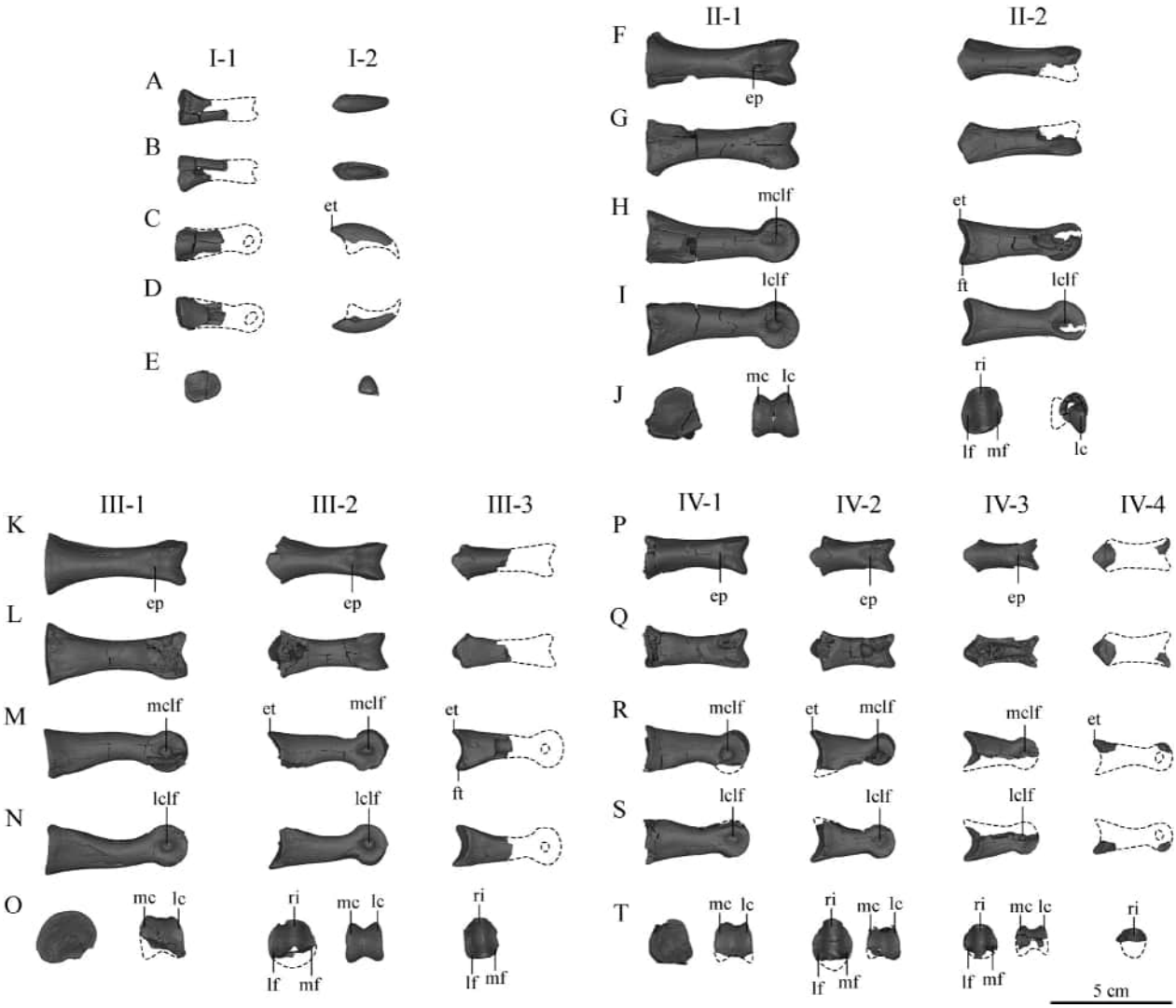

Figure 3. Digital reconstructions of pedal phalanges of referred specimen of Caudipteridae, PMOL-AD00126. Individual phalanges are labelled above each element. Phalanges of pedal digit I in dorsal (**A**), plantar (**B**), medial (**C**), lateral (**D**) and proximal (**E**) views; phalanges of pedal digit II in dorsal (**F**), plantar (**G**), medial (**H**), lateral (**I**) and proximal (left) and distal (right) (**J**) views; phalanges of pedal digit III in dorsal (**K**), plantar (**L**), medial (**M**), lateral (**N**) and proximal (left) and distal (right) (**O**) views; phalanges of pedal digit IV in dorsal (**P**), plantar (**Q**), medial (**R**), lateral (**S**) and proximal (left) and distal (right) (**T**) views. Dotted lines indicate the reconstructed outlines of the bones. Abbreviations: ep, extensor pit; et, extensor tubercle; ft, flexor tubercle; lc, lateral condyle; lclf, lateral collateral ligament fossa; lf, lateral facet; mc, medial condyle; mclf, medial collateral ligament fossa; mf, medial facet; ri, ridge.

pedal phalanges. A comparably shallow extensor pit is typical of oviraptorosaurs, such as *Anomalipes zhaoi* and *Khaan mckennai* (Balanoff and Norell 2012; Yu et al. 2018). By contrast, the extensor pit of phalanx IV-1 is markedly deeper in dromaeosaurids (Brissón Egli et al. 2017) and alvarezsauroids (Averianov and Lopatin 2021; Kubo et al. 2023). The collateral ligament fossae are deep and well-defined with an oval outline. The medial fossa is deeper than the lateral fossa, a feature also observed in *Parvicursor remotus* and *Aepyornithomimus tugrikinensis* (Chinzorig et al. 2017; Averianov and Lopatin 2021). The distal articulation is strongly ginglymoid, with a well-developed intercondylar groove (Fig. 3T). The medial condyle is slightly wider than the lateral condyle. The proximal articular surface of phalanx IV-2 is divided by a ridge into two asymmetrical facets, of which the lateral facet is slightly larger than the medial facet (Fig. 3T). The extensor tubercle is more prominent and extends more proximally than in other phalanges. The extensor pit is deep. The lateral collateral ligament fossa is noticeably shallower than its medial counterpart, a condition similar to that in *Aepyornithomimus tugrikinensis* (Chinzorig et al. 2017). The distal articulation is divided into two condyles of approximately equal size by a well-developed intercondylar groove (Fig. 3T). The proximal articular surface of phalanx IV-3 is divided by a ridge into two subequal facets (Fig. 3T). The flexor tubercle is well developed. The dorsal extensor pit is deep, but has an indistinct margin. The medial collateral ligament fossa is significantly deeper than the lateral collateral ligament fossa. The distal condyles exhibit slight transverse expansion and are separated by a well-developed intercondylar

groove (Fig. 3T). Phalanx IV-4 is largely damaged. The proximal articular surface bears a distinct median ridge and the extensor tubercle is well developed (Fig. 3T). The cast of phalanx IV-5 (ungual) is similar in size to the unguals of digits II and III and bears a lateral groove.

Histological description of metatarsal II of PMOL-AD00126

The transverse section of metatarsal II of PMOL-AD00126 exhibits an elliptical medullary cavity bounded by cortical bone of variable thickness, reaching a maximum of approximately 1.6 mm on the dorsal part of the bone wall (Fig. 4A). The innermost cortex is lined by a thin layer (61–92 μm) of endosteal bone, indicating that medullary cavity expansion was largely complete (Qin 2019). The periosteal matrix contains intrinsic fibres arranged concentrically around the long axis of the element, as indicated by the tissue birefringence and the orientation and morphology of the osteocyte lacunae. The birefringence is heterogeneous, consisting of small birefringent patches scattered throughout the matrix and several discrete areas of monorefringent tissue. This organisation differs from both fibrolamellar bone and typical parallel-fibered bone, but more closely resembles crossed parallel-fibred bone (Pereyra et al. 2020; Martínez et al. 2022). The vascular canals are predominantly longitudinally orientated and secondary osteons are scarce in PMOL-AD00126 (Fig. 4C). Two single lines of arrested growth (LAGs) are present within the cortex and a double LAG is situated between them (Fig. 4B).

Discussion

Taxonomic identification of PMOL-AD00126

In PMOL-AD00126, the proximal half of metatarsal III is pinched by metatarsals II and IV to form the subarctometatarsalian pes, a condition only known in several lineages of coelurosaurian theropods (Kubo and Kobayashi 2025). Amongst those coelurosaurian theropods, PMOL-AD00126 lacks the enlarged pedal digit II seen in deinonychosaurians (Fowler et al. 2011) and the sinusoidal profile of metatarsal III in some ornithomimosaurians (Theda et al. 2025) and tyrannosauroids (Brochu 2003). Furthermore, the longitudinal ridges on the ventral surface of metatarsal III differentiate it from non-parvicursorine alvarezsaurs such as *Alnashetri cerropoliciensis* (Makovicky et al. 2012). This suite of features suggests oviraptorosaurian affinities. However, pedal anatomy remains poorly documented amongst oviraptorosaurs from the Early Cretaceous Jehol Biota and articulated metatarsi are relatively rare amongst previously described caudipterid specimens. Based on the available comparative material, PMOL-AD00126 exhibits several pedal features resembling those of caudipterids. The proximal end of metatarsal I is positioned at approximately the distal third of metatarsal II, as in the caudipterid *Similicaudipteryx* and the oviraptorid *Ganzhousaurus* (He et al. 2008; Wang et al. 2013). In contrast, in the oviraptorid *Khaan*, metatarsal I appears to attach to metatarsal II within its distal half (Balanoff and Norell 2012). The MT I/MT II length ratio in PMOL-AD00126 is 0.19, close to that of *Similicaudipteryx* (0.17), but lower than those of *Khaan* (0.26), *Ganzhousaurus* (0.29) and the caenagnathid *Chirostenotes* (0.23) (Table 2). The Pd III-1/MT III length ratio in PMOL-AD00126 is 0.25, which falls within the range documented in caudipterids (0.21–0.30). Higher ratios occur in the caenagnathid *Citipes* (0.35), *Chirostenotes* (0.26–0.33) and the oviraptorid *Ganzhousaurus* (0.31) (Table 2). The Pd II-1/Pd III-1 ratio of PMOL-AD00126 is about 1.06, which is close to those in *Xingtianosaurus* (1.05), *Citipes* (1.05) and *Chirostenotes* (1.04). It is higher than those of *Khaan* (0.95) and *Ganzhousaurus* (0.91). The MT III W25/W75 ratio of PMOL-AD00126 is 0.51, indicating an intermediate degree of proximal constriction between the lower ratios observed in *Avimimus* (0.07), *Citipes* (0.30) and *Chirostenotes* (0.42) and the higher ratios in *Khaan* (0.74) and *Ganzhousaurus* (0.70) (Table 2; Snively et al. (2004)).

In addition, the proximal ends of metatarsals II and IV remain unfused, as in known caudipterid specimens and the oviraptorid *Wulatelong* (Zhou et al. 2000; He et al. 2008; Xu et al. 2013; Qiu et al. 2019). In contrast, the proximal tarsometatarsus shows varying degrees of fusion and a more pronounced arctometatarsalian condition in *Avimimus*, *Yuanyanglong* and some caenagnathids (Funston et al. 2016; Funston et al. 2019; Hao et al. 2025). PMOL-AD00126 lacks tibiotarsal fusion, as in *Caudipteryx*, *Xingtianosaurus*, *Khaan* and *Chirostenotes*, but unlike the fused condition in *Yuanyanglong* and adult *Avimimus* (Ji et al. 1998; Balanoff and Norell 2012; Funston et al. 2019; Qiu et al. 2019; Funston and Currie 2021; Hao et al. 2025).

Although no individual pedal feature of PMOL-AD00126 can currently be regarded as an unambiguous synapomorphy of Caudipteridae, the combination of these features closely matches the pedal morphology documented in caudipterids, including *Caudipteryx*, *Similicaudipteryx* and *Xingtianosaurus*. This combination, therefore, supports the provisional referral of PMOL-AD00126 to Caudipteridae.

Newly-discovered features of Caudipteridae from PMOL-AD00126

The new caudipterid specimen described here (PMOL-AD00126) exhibits several previously unreported osteological features, including: (a) metatarsal III is fully

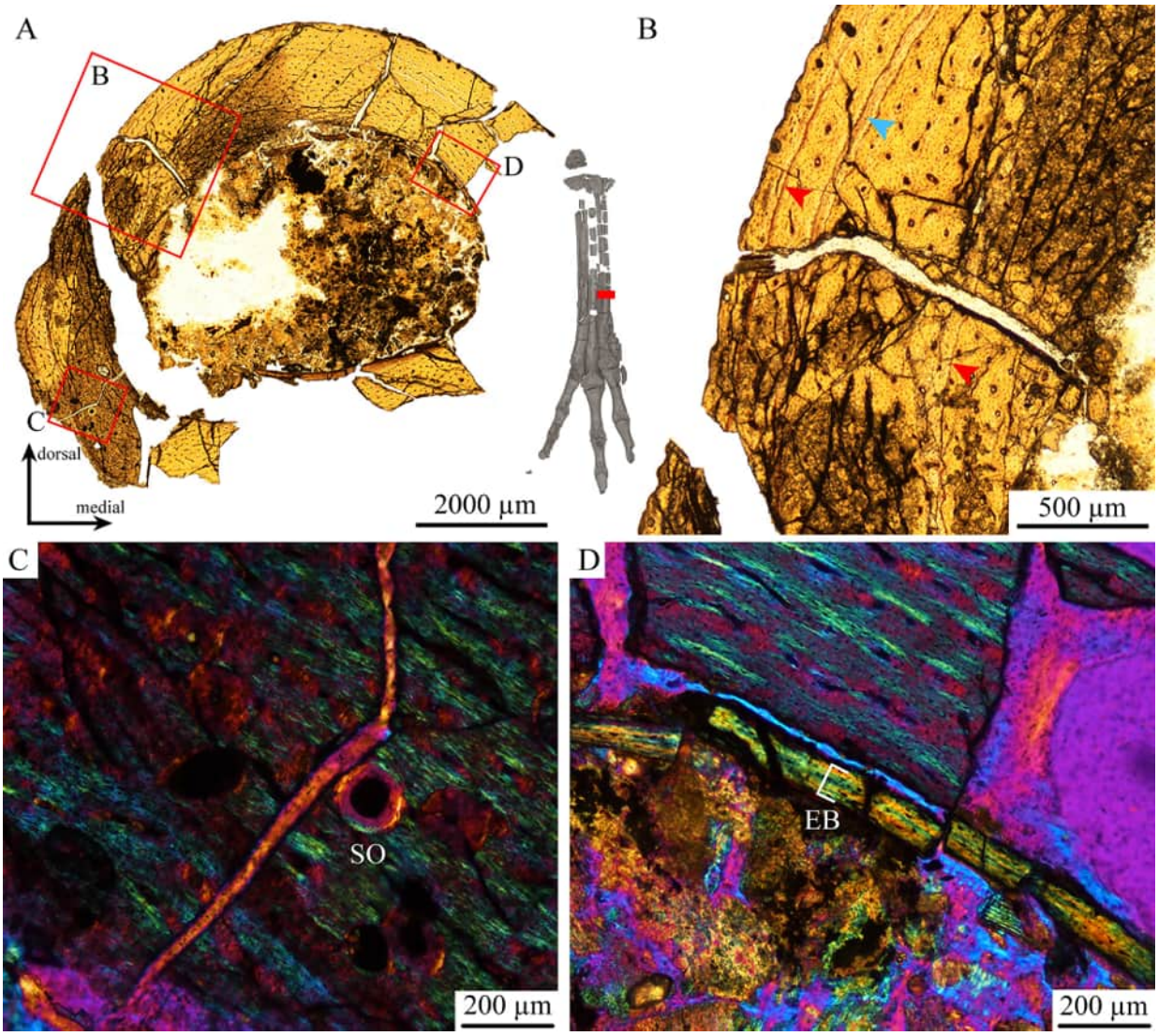

Figure 4. Osteohistology of metatarsal II of PMOL-AD00126. Thin section imaged under normal light (**A**), with red boxes indicating the locations of the magnified regions shown in (**B–D**); lines of arrested growth (normal light) (**B**); secondary osteon (polarised light) (**C**); inner circumferential lamellae (polarised light) (**D**). The grey digital reconstruction shows the pes in ventral view and the red mark indicates the level of the transverse section through the mid-distal portion of metatarsal II. The red arrow indicates the lines of arrested growth and the blue arrow indicates the double lines of arrested growth. Abbreviations: EB, endosteal bone; SO, secondary osteon. Scales as indicated.

exposed dorsally, forming a subarctometatarsalian condition; (b) the mid-shaft of metatarsal I bears pronounced dorsal and plantar prominences and a spherical distal articulation; (c) a distinct posteromedial ridge extends along the plantar surface of metatarsal II; (d) a proximodistally elongated extensor pit is present on the dorsal surface of metatarsal III; (e) two longitudinal ridges on the plantar surface of metatarsal III are separated from the plantar condylar ridges of the distal articulation by a shallow groove; (f) all preserved distal phalanges bear deep extensor ligament pits on their dorsal surfaces; (g) the proximal articular surfaces of the first phalanx of each digit are a single cavity and lack a ridge, whereas the proximal articular surfaces of the remaining phalanges are divided by a ridge.

Evolution of the metatarsal arrangement in Oviraptorosauria

Within Oviraptorosauria, metatarsal morphology shows considerable variation (Fig. 5). A plesiomorphic, non-arctometatarsalian metatarsus occurs in the earliest-diverging oviraptorosaur *Protarchaeopteryx robusta* (Ji and Ji 1997), most oviraptorids (e.g. *Ganzhousaurus nankangensis*, *Rinchenia mongoliensis*, *Citipati osmolskae* and *Khaan mckennai*) and the caenagnathid *Gigantoraptor erlianensis* (Xu et al. 2007; Balanoff and Norell 2012; Wang et al. 2013; Funston et al. 2018; Norell et al. 2018). By contrast, an arctometatarsalian condition characterises *Avimimus portentosus* and most caenagnathids (Vickers-Rich et al. 2002; Currie et al. 2016; Yu et al. 2018).

Table 2. Comparison of pedal character states among PMOL-AD00126 and other oviraptorosaurian specimens with well-preserved pedal elements.

Group	Taxon	Attachment of MT I on MT II	MT I/MT II length ratio	Pd III-1/MT III length ratio	Pd II-1/Pd III-1 length ratio	MT III anterior width ratio W25/W75 *	Proximal exposure of MT III	Proximal tarsometatarsal fusion	Tibiotarsal fusion	References
Caudipterids	**PMOL-AD00126[a]**	~distal 1/3	0.19	0.25	1.06	0.51	Yes	No	No	This study
	Caudipteryx zoui	~distal 1/4	0.16	0.21	0.96	?	Yes	No	No	Zhou et al. (2000)
	Similicaudipteryx yixianensis	~distal 1/3	0.17	0.25	0.93	?	?	No	?	He et al. (2008)
	Xingtianosaurus ganqi	~distal 1/4	0.12	0.30	1.05	?	?	No	No	Qiu et al. (2019)
Non-caudipterid oviraptorosaurians	*Protarchaeopteryx robusta*	~distal 1/2	~0.17	~0.21	~0.89	?	?	No	?	Ji et al. (1998)
	Avimimus nemegtensis	?	?	?	?	0.07	No	Yes (adult)	Yes (adult)	Funston et al. (2019)
	Yuanyanglong bainian	?	?	?	?	?	No	Yes	Yes	Hao et al. (2025)
	Khaan mckennai	~distal 1/2	0.26	0.28	0.95	0.74	Yes	No	No	Balanoff and Norell (2012)
	Ganzhousaurus nankangensis	~distal 1/3	0.29	0.31	0.91	0.70	Yes	No	?	Wang et al. (2013)
	Citipes elegans	?	?	0.35	1.05	0.30	No	Yes	?	Funston et al. (2016)
	Chirostenotes pergracilis	~distal 1/5	0.23	0.26–0.33	1.04	0.42	No	No	No	Funston and Currie (2021)

Abbreviations: MT, metatarsal; Pd, pedal phalanx. Symbols: ~, approximate value; ?, indeterminate (preservation or data unavailable). * Ratio of the anteriorly exposed width of MT III at 25% and 75% of its proximodistal length (W25/W75); measurements of W25 and W75 follow Snively et al. (2004). [a] PMOL-AD00126 is provisionally referred to Caudipteridae.

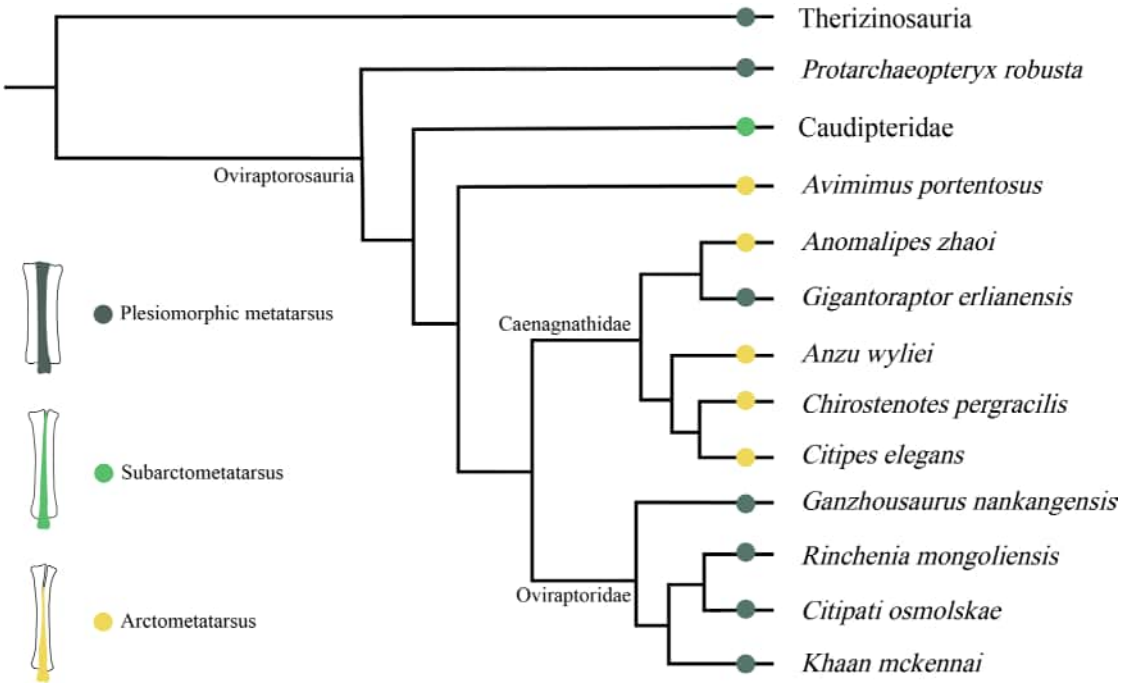

Figure 5. Phylogenetic diagram and metatarsal arrangement of Oviraptorosauria. A simplified phylogenetic tree modified from Yu et al. (2018).

In this broader comparative context, the exact metatarsal arrangement in Caudipteridae has remained uncertain. Although lateral compression of metatarsal III has been reported in caudipterids (Zhou and Wang 2000; Qiu et al. 2019; Hao et al. 2025), the absence of fully exposed *in situ* metatarsals in previously described specimens has precluded a definitive assessment of the metatarsal arrangement.

The identification of a subarctometatarsalian condition in PMOL-AD00126 resolves the long-standing

ambiguity regarding the exact metatarsal arrangement in Caudipteridae. This also represents the first discovery of a subarctometatarsus in Oviraptorosauria. The arctometatarsus is interpreted as a mechanically reinforced metatarsal structure that is adapted for terrestrial locomotion (Holtz 1995; Kubo and Kobayashi 2025). The subarctometatarsalian condition is widely regarded as intermediate between the plesiomorphic metatarsus and the arctometatarsalian condition. This finding indicates a trend towards enhanced cursorial capability in some early-diverging oviraptorosaurs and suggests that later-diverging oviraptorosaurs underwent a more complex locomotor evolution.

Osteohistological inferences on maturity of PMOL-AD00126

In the bone matrix of PMOL-AD00126, the vascular canals are predominantly longitudinally orientated. This vascular organisation contrasts with that observed in metatarsal II of the caenagnathid specimen TMP 1990.52.10, which exhibits denser vascularisation, characterised by reticular and plexiform canals (Voris et al. 2024).

Although the number of LAGs cannot be regarded as a straightforward proxy for chronological age (Chinsamy and Pereyra 2026), the decrease in vascular density and progressive narrowing of LAG spacing towards the periosteum are consistent with increasing somatic maturity (Guo et al. 2026; Makovicky et al. 2026). Nevertheless, the absence of an external fundamental system (EFS) together with the retention of abundant vascularity in the outermost cortex indicate that complete somatic maturity had not been attained.

The total pes length (MT III + pedal digit III) of PMOL-AD00126 is 216.4 mm, which exceeds that of most known caudipterid specimens (e.g. *Xingtianosaurus ganqi* holotype specimen, 175.1 mm and *Caudipteryx dongi* holotype specimen, 208 mm) (Zhou and Wang 2000; Qiu et al. 2019). However, it is substantially shorter than that of the holotype of *Similicaudipteryx yixianensis* (329 mm) (He et al. 2008) and the referred specimen PMOL-AD00113 (MT III of PMOL-AD00113 = 162 mm; PMOL-AD00126 = 118.5 mm) (Table 1) (Liu 2014). We refrain from assigning PMOL-AD00126 to either *Caudipteryx dongi* or *Similicaudipteryx yixianensis* solely based on pedal skeletal size, as the somatic maturity of other caudipterid specimens remains unclear. A deeper understanding of the osteohistological data of early oviraptorosaurs is crucial not only for resolving the taxonomic assignment of PMOL-AD00126, but also for reassessing the taxonomic validity of early oviraptorosaur species reported from the Jehol Biota, because many diagnostic traits rely on skeletal proportions that may be influenced by allometry.

Conclusions

The new caudipterid pedal specimen, PMOL-AD00126, reveals several previously unrecognised osteological features, most notably a subarctometatarsalian condition, which represents the first unambiguous evidence of this condition in oviraptorosaurs. These features add to the current understanding of the sequence of pedal modifications and provide new anatomical data that can inform future functional studies of terrestrial locomotion, including aspects related to cursorial ability, digit extension, foot stabilisation and postural control. Osteohistological analysis further indicates that this individual had not attained complete somatic maturity. Together, the osteological and histological evidence presented here contributes new information relevant to pedal evolution and ontogeny in early oviraptorosaurs.

Acknowledgements

We thank Yemao Hou, Pengfei Yin and Jia Wang for assistance with computed tomography scanning; Jingqi Wang for collection management; Liang Jiao for photography; and Shurui Yang for preparing the specimen.

References

Atkins-Weltman KL, Simon DJ, Woodward HN, Funston GF, Snively E (2024) A new oviraptorosaur (Dinosauria: Theropoda) from the end-Maastrichtian Hell Creek Formation of North America. PLoS ONE 19(1): e0294901. https://doi.org/10.1371/journal.pone.0294901

Averianov AO, Lopatin AV (2021) A re-appraisal of *Parvicursor remotus* from the Late Cretaceous of Mongolia: implications for the phylogeny and taxonomy of alvarezsaurid theropod dinosaurs. Journal of Systematic Palaeontology 19(16): 1097–1128. https://doi.org/10.1080/14772019.2021.2013965

Balanoff AM, Norell MA (2012) Osteology of *Khaan mckennai* (Oviraptorosauria: Theropoda). Bulletin of the American Museum of Natural History (372): 1–77. https://doi.org/10.1206/803.1

Bi S, Amiot R, Peyre de Fabrègues C, Pittman M, Lamanna MC, Yu Y, Yu C, Yang T, Zhang S, Zhao Q, Xu X (2021) An oviraptorid preserved atop an embryo-bearing egg clutch sheds light on the reproductive biology of non-avialan theropod dinosaurs. Science Bulletin 66(9): 947–954. https://doi.org/10.1016/j.scib.2020.12.018

Brissón Egli F, Aranciaga Rolando AM, Agnolin FL, Novas FE (2017) Osteology of the unenlagiid theropod *Neuquenraptor argentinus* from the Late Cretaceous of Patagonia. Acta Palaeontologica Polonica 62(3): 549–562. https://doi.org/10.4202/app.00348.2017

Brochu CA (2003) Osteology of *Tyrannosaurus rex*: insights from a nearly complete skeleton and high-resolution computed tomographic analysis of the skull. Journal of Vertebrate Paleontology 22(sup4): 1–138. https://doi.org/10.1080/02724634.2003.10010947

Chinsamy A, Pereyra M-E (2026) Stochastic growth marks in *Crocodylus niloticus*. Scientific Reports 16(1): 1811. https://doi.org/10.1038/s41598-025-31384-5

Chinzorig T, Kobayashi Y, Tsogtbaatar K, Currie PJ, Watabe M, Barsbold R (2017) First ornithomimid (Theropoda, Ornithomimosauria) from the Upper Cretaceous Djadokhta Formation of Tögrögiin Shiree, Mongolia. Scientific Reports 7(1): 5835. https://doi.org/10.1038/s41598-017-05272-6

Cullen TM, Canale JI, Apesteguía S, Smith ND, Hu D, Makovicky PJ (2020) Osteohistological analyses reveal diverse strategies of theropod dinosaur body-size evolution. Proceedings of the Royal Society B: Biological Sciences 287(1939): 20202258. https://doi.org/10.1098/rspb.2020.2258

Currie PJ (1989) The first records of *Elmisaurus* (Saurischia, Theropoda) from North America. Canadian Journal of Earth Sciences 26(6): 1319–1324. https://doi.org/10.1139/e89-111

Currie PJ, Funston GF, Osmólska H (2016) New specimens of the crested theropod dinosaur *Elmisaurus rarus* from Mongolia. Acta Palaeontologica Polonica 61(1): 143–157. https://doi.org/10.4202/app.00130.2014

Erickson GM, Rauhut OWM, Zhou Z, Turner AH, Inouye BD, Hu D, Norell MA (2009) Was dinosaurian physiology inherited by birds? Reconciling slow growth in *Archaeopteryx*. PLoS ONE 4(10): e7390. https://doi.org/10.1371/journal.pone.0007390

Fowler DW, Freedman EA, Scannella JB, Kambic RE (2011) The predatory ecology of *Deinonychus* and the origin of flapping in birds. PLoS ONE 6(12): e28964. https://doi.org/10.1371/journal.pone.0028964

Funston GF (2020) Caenagnathids of the Dinosaur Park Formation (Campanian) of Alberta, Canada: anatomy, osteohistology, taxonomy, and evolution. Vertebrate Anatomy Morphology Palaeontology 8: 105–153. https://doi.org/10.18435/vamp29362

Funston GF, Currie PJ (2021) New material of *Chirostenotes pergracilis* (Theropoda, Oviraptorosauria) from the Campanian Dinosaur Park Formation of Alberta, Canada. Historical Biology 33(9): 1671–1685. https://doi.org/10.1080/08912963.2020.1726908

Funston GF, Persons IV WS, Bradley GJ, Currie PJ (2015) New material of the large-bodied caenagnathid *Caenagnathus collinsi* from the Dinosaur Park Formation of Alberta, Canada. Cretaceous Research 54: 179–187. https://doi.org/10.1016/j.cretres.2014.12.002

Funston GF, Currie PJ, Burns ME (2016) New elmisaurine specimens from North America and their relationship to the Mongolian *Elmisaurus rarus*. Acta Palaeontologica Polonica 61(1): 159–173. https://doi.org/10.4202/app.00129.2014

Funston GF, Mendonca SE, Currie PJ, Barsbold R (2018) Oviraptorosaur anatomy, diversity and ecology in the Nemegt Basin. Palaeogeography, Palaeoclimatology, Palaeoecology 494: 101–120. https://doi.org/10.1016/j.palaeo.2017.10.023

Funston GF, Currie PJ, Ryan MJ, Dong Z-M (2019) Birdlike growth and mixed-age flocks in avimimids (Theropoda, Oviraptorosauria). Scientific Reports 9(1): 18816. https://doi.org/10.1038/s41598-019-55038-5

Guo T, He Y, Zhao Q (2026) Osteohistology on *Liaoceratops yanzigouensis* (Dinosauria: Neoceratopsia) from the Early Cretaceous Jehol Biota. Vertebrata Palasiatica 64(3): 221–237. https://doi.org/10.19615/j.cnki.2096-9899.250708

Hao M, Li Z, Wang Z, Wang S, Ma F, Qinggele, King JL, Pei R, Zhao Q, Xu X (2025) A new oviraptorosaur from the Lower Cretaceous Miaogou Formation of western Inner Mongolia, China. Cretaceous Research 167: 106023. https://doi.org/10.1016/j.cretres.2024.106023

Hattori S (2016) Evolution of the hallux in non-avian theropod dinosaurs. Journal of Vertebrate Paleontology 36(4): e1116995. https://doi.org/10.1080/02724634.2016.1116995

He T, Wang X, Zhou Z (2008) A new genus and species of caudipterid dinosaur from the Lower Cretaceous Jiufotang Formation of western Liaoning, China. Vertebrata Palasiatica 46(3): 178–189.

Hendrickx C, Hartman SA, Mateus O (2015) An overview of non-avian theropod discoveries and classification. PalArch's Journal of Vertebrate Palaeontology 12(1): 1–73.

Holtz TR (1995) The arctometatarsalian pes, an unusual structure of the metatarsus of Cretaceous Theropoda (Dinosauria: Saurischia). Journal of Vertebrate Paleontology 14(4): 480–519. https://doi.org/10.1080/02724634.1995.10011574

Ji Q, Ji S-A (1997) A Chinese archaeopterygian, *Protarchaeopteryx* gen. nov. Geological Science and Technology 238: 38–41.

Ji Q, Currie PJ, Norell MA, Ji S-A (1998) Two feathered dinosaurs from northeastern China. Nature 393: 753–761. https://doi.org/10.1038/31635

Ji Q, Lv J, Wei X, Wang X (2012) A new oviraptorosaur from the Yixian Formation of Jianchang, western Liaoning Province, China. Geological Bulletin of China 31(12): 2102–2107.

Kubo K, Kobayashi Y (2025) Cursorial ecomorphology and temporal patterns in theropod dinosaur evolution during the mid-Cretaceous. Royal Society Open Science 12(1): 241178. https://doi.org/10.1098/rsos.241178

Kubo K, Kobayashi Y, Chinzorig T, Tsogtbaatar K (2023) A new alvarezsaurid dinosaur (Theropoda, Alvarezsauria) from the Upper Cretaceous Baruungoyot Formation of Mongolia provides insights for bird-like sleeping behavior in non-avian dinosaurs. PLoS ONE 18(11): e0293801. https://doi.org/10.1371/journal.pone.0293801

Liu D (2014) New material of *Similicaudipteryx* from the Lower Cretaceous of western Liaoning. Master's Thesis, Shenyang Normal University, Shenyang.

Makovicky PJ, Apesteguía S, Gianechini FA (2012) A new coelurosaurian theropod from the La Buitrera fossil locality of Río Negro, Argentina. Fieldiana Life and Earth Sciences 2012(5): 90–98. https://doi.org/10.3158/2158-5520-5.1.90

Makovicky PJ, Mitchell JS, Meso JG, Gianechini FA, Cerda I, Apesteguía S (2026) Argentine fossil rewrites evolutionary history of a baffling dinosaur clade. Nature 652: 1240–1244. https://doi.org/10.1038/s41586-026-10194-3

Martínez RN, Andres B, Apaldetti C, Cerda IA (2022) The dawn of the flying reptiles: first Triassic record in the southern hemisphere. Papers in Palaeontology 8(2): e1424. https://doi.org/10.1002/spp2.1424

Norell MA, Balanoff AM, Barta DE, Erickson GM (2018) A second specimen of *Citipati osmolskae* associated with a nest of eggs from Ukhaa Tolgod, Omnogov Aimag, Mongolia. American Museum Novitates 3899: 1–44. https://doi.org/10.1206/3899.1

Osmólska H (1981) Coossified tarsometatarsi in theropod dinosaurs and their bearing on the problem of bird origins. Palaeontologia Polonica 42: 79–95.

Padian K, Lamm E-T [Eds] (2013) Bone histology of fossil tetrapods: advancing methods, analysis, and interpretation. University of California Press, Berkeley. https://doi.org/10.1525/9780520955110

Pereyra ME, Bona P, Cerda IA, Jannello JM, De La Fuente MS, Desántolo B (2020) Growth dynamics and body size evolution of South American long-necked chelid turtles: A bone histology approach. Acta Palaeontologica Polonica 65(3): 535–545. https://doi.org/10.4202/app.00702.2019

Qin Z-C (2019) A new middle-Late Jurassic alvarezsaurians from Shishugou Formation, Xinjiang, China, and the study of histology and body size evolution of alvarezsaurians. Master's Thesis, University of Chinese Academy of Sciences, Beijing.

Qin Z-C, Zhao Q, Xu X (2019) Metatarsal II osteohistology of *Xixianykus zhangi* (Theropoda: Alvarezsauria) and its implications for the development of the arctometatarsalian pes. Vertebrata Palasiatica 57(3): 205–213. https://doi.org/10.19615/j.cnki.1000-3118.190425

Qiu R, Wang X, Wang Q, Li N, Zhang J, Ma Y (2019) A new caudipterid from the Lower Cretaceous of China with information on the evolution of the manus of Oviraptorosauria. Scientific Reports 9(1): 6431. https://doi.org/10.1038/s41598-019-42547-6

Snively E, Russell AP, Powell GL (2004) Evolutionary morphology of the coelurosaurian arctometatarsus: descriptive, morphometric and phylogenetic approaches. Zoological Journal of the Linnean Society 142(4): 525–553. https://doi.org/10.1111/j.1096-3642.2004.00137.x

Theda D, Nau D, Dederichs R, Schwermann AH (2025) The first ornithomimosaur remains from Germany. Acta Palaeontologica Polonica 70(3): 543–555. https://doi.org/10.4202/app.01262.2025

Tsogtbaatar C, Cullen T, Phillips G, Rolke R, Zanno LE (2022) Large-bodied ornithomimosaurs inhabited Appalachia during the Late Cretaceous of North America. PLoS ONE 17(10): e0266648. https://doi.org/10.1371/journal.pone.0266648

Tsujimura K, Manabe M, Chiba Y, Tsuihiji T (2021) Metatarsals of a large caenagnathid cf. *Anzu wyliei* (Theropoda: Oviraptorosauria) from the Hell Creek Formation in South Dakota, USA. Canadian Journal of Earth Sciences 58(9): 911–917. https://doi.org/10.1139/cjes-2020-0171

Vickers-Rich P, Chiappe LM, Kurzanov S (2002) The enigmatic birdlike dinosaur *Avimimus portentosus*: comments and a pictorial atlas. In: Chiappe LM, Witmer LM (Eds) Mesozoic Birds: Above the Heads of Dinosaurs. University of California Press, Berkeley, 65–86.

Voris JT, Zelenitsky DK, Therrien F (2024) Caenagnathids (Theropoda, Oviraptorosauria) from the uppermost Maastrichtian of the Scollard Formation of Alberta, Canada. Cretaceous Research 153: 105708. https://doi.org/10.1016/j.cretres.2023.105708

Wang S, Sun C, Sullivan C, Xu X (2013) A new oviraptorid (Dinosauria: Theropoda) from the Upper Cretaceous of southern China. Zootaxa 3640(2): 242–257. https://doi.org/10.11646/zootaxa.3640.2.7

White MA, Cook AG, Klinkhamer AJ, Elliott DA (2016) The pes of *Australovenator wintonensis* (Theropoda: Megaraptoridae): analysis of the pedal range of motion and biological restoration. PeerJ 4: e2312. https://doi.org/10.7717/peerj.2312

Wu Q, Bailleul AM, Li Z, O'Connor J, Zhou Z (2021) Osteohistology of the scapulocoracoid of *Confuciusornis* and preliminary analysis of the shoulder joint in Aves. Frontiers in Earth Science 9: 617124. https://doi.org/10.3389/feart.2021.617124

Wu Q, Pan Y, Li Z, Zhou Z, Bailleul AM (2024) First histochemical examination of a Miocene ostrich eggshell with the oldest mineral-bound peptides. Vertebrata Palasiatica 62(2): 120–134. https://doi.org/10.19615/j.cnki.2096-9899.240329

Wu Q, Chen H, Li Z, Jiang S, Wang X, Zhou Z (2025) The morphology and histology of the pectoral girdle of *Hamipterus* (Pterosauria), from the Early Cretaceous of Northwest China. The Anatomical Record 308(10): 2630–2641. https://doi.org/10.1002/ar.25167

Xu X, Tan Q, Wang J, Zhao X, Tan L (2007) A gigantic bird-like dinosaur from the Late Cretaceous of China. Nature 447(7146): 844–847. https://doi.org/10.1038/nature05849

Xu X, Tan Q-W, Wang S, Sullivan C, Hone DWE, Han F-L, Ma Q-Y, Tan L, Xiao D (2013) A new oviraptorid from the Upper Cretaceous of Nei Mongol, China, and its stratigraphic implications. Vertebrata Palasiatica 51(2): 85–101.

Yu Y, Wang K, Chen S, Sullivan C, Wang S, Wang P, Xu X (2018) A new caenagnathid dinosaur from the Upper Cretaceous Wangshi Group of Shandong, China, with comments on size variation among oviraptorosaurs. Scientific Reports 8(1): 5030. https://doi.org/10.1038/s41598-018-23252-2

Yun C-G, Funston GG (2021) A caenagnathid oviraptorosaur metatarsal from the Mesaverde Formation (Campanian), Wyoming. Vertebrate Anatomy Morphology Palaeontology 9(1): 105–115. https://doi.org/10.18435/vamp29376

Zhou Z, Wang X (2000) A new species of *Caudipteryx* from the Yixian Formation of Liaoning, northeast China. Vertebrata Palasiatica 38(2): 111–127.

Zhou Z, Wang X, Zhang F, Xu X (2000) Important features of *Caudipteryx*-evidence from two nearly complete new specimens. Vertebrata Palasiatica 38(4): 241–254.

Additional information

Conflict of interest

The authors have declared that no competing interests exist.

Ethical statement

No ethical statement was reported.

Artificial Intelligence (AI) use

The authors accept full responsibility for the content of the manuscript, including the disclosure of any use of AI.
No AI tools were used in the preparation of this manuscript.

Funding

This work was supported by the National Natural Science Foundation of China (Grant Nos. 42402017 to W.S., 42502005 to L.Y. and 42302012 to W. Q.), the Research Fund for International Scientists of the National Natural Science Foundation of China (Grant No. 42350410443, awarded to P.R.) and the Liaoning Provincial Natural Science Foundation (Grant Nos. 2025-BS-0797 to W.S. and 2025-MSLH-621 to S.S.).

Author contributions

Conceptualization: MH, MD, SW. Investigation: MH, MD, SS, QW, SW. Project administration: SW. Resources: SW. Visualization: MH, MD, SW. Writing – original draft: MH, MD, SW. Writing – review and editing: MH, MD, JS, MZH, YJL, SS, KK, YL, QW, PR, SW.

Author ORCIDs

M. Han https://orcid.org/0009-0000-1570-9520
M. Duan https://orcid.org/0009-0007-0735-5110
M. Hao https://orcid.org/0009-0004-4117-715X
Y. Liu https://orcid.org/0009-0001-0102-0869
K. Kubo https://orcid.org/0009-0006-5336-4379
Q. Wu https://orcid.org/0000-0001-7646-8329
P. Rummy https://orcid.org/0000-0002-8552-9848
S. Wang https://orcid.org/0000-0001-6067-0303

Data availability

The deposited dataset comprises a micro-CT image stack in TIFF format, segmented three-dimensional models of the individual pedal elements in STL format and a README file. The dataset is available in ScienceDB at https://www.scidb.cn/anonymous/WVozWW55.